Supplemental Material: The double-edge sword of disorder in multichannel topological superconductors

Arbel Haim[1] and Ady Stern[2]
[1] *Walter Burke Institute for Theoretical Physics and the Institute for Quantum Information and Matter, California Institute of Technology, Pasadena, CA 91125, USA*
[2] *Department of Condensed Matter Physics, Weizmann Institute of Science, Rehovot 7610001, Israel*

CONTENTS

I. DETAILS OF NUMERICAL SIMULATIONS

In this section we present details of the numerical simulations whose results are summarized in Fig. 1 of the main text. We begin by presenting the lattice model used for simulating the system. We then explain the procedure for obtaining the reflection matrix and extracting the Majorana localization length.

A. The lattice model

For the purpose of numerically simulating the planar Josephson junction [Eq. (1) of the main text], we replace it with a model of a $N_x \times N_y$ square lattice of lattice constant a, whose Hamiltonian is given by

$$H_{\mathrm{PJJ}} = \sum_{n_x=1}^{N_x}\sum_{n_y=1}^{N_y}\sum_{s,s'\in\{\uparrow,\downarrow\}}\Big\{[(U_{n_x,n_y}-\mu_{n_y})\sigma^0_{ss'} - E^{\mathrm{Z}}_{n_y}\sigma^x_{ss'}]c^\dagger_{\boldsymbol{n},s}c_{\boldsymbol{n},s'} - \sum_{\boldsymbol{d}\in\{\pm\hat{x},\pm\hat{y}\}}[t_0\sigma^0_{ss'} + iu(\boldsymbol{\sigma}_{ss'}\times\boldsymbol{d})\cdot\hat{z}]c^\dagger_{\boldsymbol{n},s}c_{\boldsymbol{n}+\boldsymbol{d},s'} + \frac{1}{2}[\Delta_{n_y}i\sigma^y_{ss'}c^\dagger_{\boldsymbol{n},s}c^\dagger_{\boldsymbol{n},s'} + \mathrm{h.c.}]\Big\} \tag{1}$$

where $c^\dagger_{\boldsymbol{n},s}$ creates an electron on site $\boldsymbol{n} = (n_x, n_y)$, $U_{n_x,n_y} = U(n_x a, n_y a)$, $\mu_{n_y} = \mu(n_y a) - 4t_0$, $E^{\mathrm{Z}}_{n_y} = E_{\mathrm{Z}}(n_y a)$, $\Delta_{n_y} = \Delta(n_y a)$, $t_0 = 1/2m_{\mathrm{e}}a^2$, $u = \alpha/2a$, $N_x = L_x/a$, and $N_y = (2W_{\mathrm{sc}} + W)/a$. In the present work, we use $t_0 = 2.5$.

B. The reflection matrix

We begin by rewriting the Hamiltonian in the following form

$$H_{\rm PJJ} = \sum_{n_x=1}^{N_x} \vec{\psi}^\dagger_{n_x} h_{n_x} \vec{\psi}_{n_x} + \left[\vec{\psi}^\dagger_{n_x} V \vec{\psi}_{n_x+1} + \text{h.c.}\right], \tag{2}$$

where $\vec{\psi}^\dagger_{n_x} = (c^\dagger_{n_x,1,\uparrow}, c_{n_x,1,\uparrow}, c^\dagger_{n_x,1,\downarrow}, c_{n_x,1,\downarrow}, \ldots, c^\dagger_{n_x,N_y,\uparrow}, c_{n_x,N_y,\uparrow}, c^\dagger_{n_x,N_y,\downarrow}, c_{n_x,N_y,\downarrow})$ is a $1\times 4N_y$ vector of creation and annihilation operators, and where $\{h_{n_x}\}_{n_x=1}^{N_x}$ and V are $4N_y \times 4N_y$ matrices.

We place two normal-metal leads, at $x=0$ and $x=L_x$. The reflection matrix for electrons and holes incident from the right is given by [1, 2]

$$r(\omega) = \mathbb{1} - 2\pi i W_{\rm R}^\dagger [G^{-1}_{N_x}(\omega) + i\pi W_{\rm R} W_{\rm R}^\dagger] W_{\rm R}, \tag{3}$$

where $W_{\rm R} \equiv \sqrt{\rho_{\rm R}} V$, with $\rho_{\rm R}$ being the density of states in the right lead, and G_{N_x} is the Green function matrix at the right-most sites of the system, obtained through the recursive relation [3]

$$G_{n_x}(\omega) = [\omega - h_{n_x} - V^\dagger G_{n_x-1} V]^{-1}. \tag{4}$$

Here, $G_{n_x}(\omega)$ is a $4N_y \times 4N_y$ matrix for every n_x (indices running over spin, particle-hole and n_y), and $G_0 = -i\pi\rho_{\rm L}$, with $\rho_{\rm L}$ being the density of states in the left lead.

C. Topological invariant and localization length

Given the reflection matrix, the topological invariant is given by [4, 5] $\mathcal{Q} = \lim_{N_x\to\infty} \det[r(0)]$, which takes the value $+1$ (-1) in the trivial (topological) phase. As an example, in Fig. 1(a) we present $\det[r(0)]$ as a function of system's length, N_x, for four different disorder realizations, with increasing value of disorder strength. The rest of the system parameters are as in Fig. 1 of the main text, with $E_{\rm Z,J} = 1$ and $\phi = \pi$. When calculating the topological invariant for a clean system [Fig. 1(a) of the main text] we have instead used the Pfaffian invariant introduced in Ref. [6].

To obtain the localization length, the transmission probability matrix is obtained through $T(\omega) \equiv t^\dagger(\omega) t(\omega) = 1 - r^\dagger(\omega) r(\omega)$, where $t(\omega)$ is the transmission matrix, and we used the fact that the scattering matrix is unitary. The Majorana localization length is determined by the decay of the largest eigenvalue of $T(0)$. This eigenvalue is shown in Fig. 1(b) as a function of N_x for four different value of disorder strength. We then extract the localization length by computing

$$\xi = a \sum_{N_x=1}^{N_x^{\rm max}\to\infty} T_{\rm max}(\omega = 0, N_x a), \tag{5}$$

where by $T_{\rm max}(\omega, L_x)$ we denote the largest eigenvalue of the transmission probability, for a system of length L_x. Notice that for an exponentially decaying transmission, $T_{\rm max}(0, L_x) = \exp(-\lambda L_x)$, this indeed yields the decay length, $\xi = 1/\lambda$, assuming the lattice spacing is taking to be small enough ($a \ll \xi$). In the simulations presented in this work we averaged ξ over a 100 realizations for every data point, and the maximal system's length was $N_x^{\rm max} = 10^4$.

Finally, in Fig. 1(c) we present the x profile of the zero-energy local density of states, $\rho(x) \equiv \int {\rm d}y \mathcal{N}(\omega = 0, x, y)$, for the four disorder realizations corresponding to Figs. 1(a) and 1(b). The local density of states, $\mathcal{N}(\omega, x, y)$, was calculated according to the method described in Ref. [7].

D. results for different parameters

In Fig. 2, we present results for a junction with parameters different from those shown in Fig. 1 of the main text. Figure 2(a) presents the phase diagram in the clean limit, and Fig. 2(b) presents the Majorana localization length as a function of disorder strength, for chemical potential $\mu_{\rm J} = \mu_{\rm sc} = 0.5$. The rest of the parameters are the same as in Fig. 1 of the main text. The same qualitative behavior is observed as in Fig. 1 of the main text.

In Fig. 2(c) we examine the effect of disorder on the system's phase diagram, for $\mu_{\rm J} = \mu_{\rm sc} = 1$, and for a narrower junction, $W = 2.5 l_{\rm so}$ (compared with $W = 5 l_{\rm so}$ in the main text). The rest of the system parameters are the same

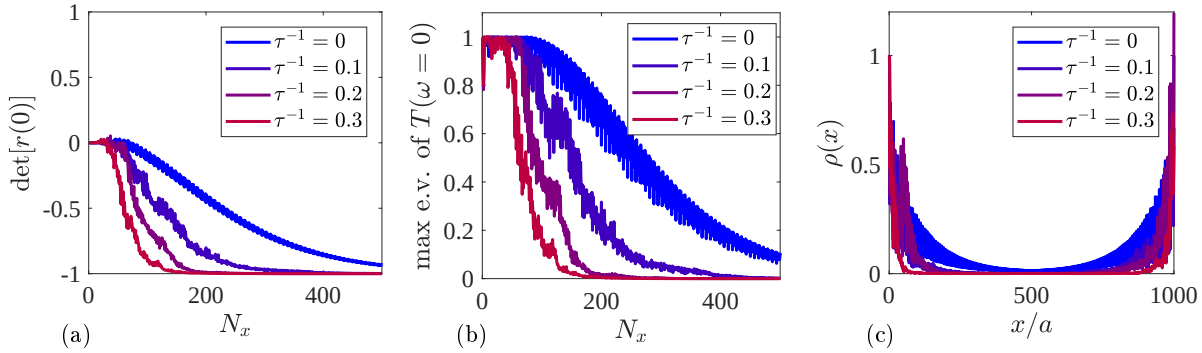

Figure 1. (a) The topological invariant, $\mathcal{Q} = \det[r(\omega = 0)]$ as a function of the system's length, $N_x = L_x/a$, for different disorder strength, characterized by the inverse mean free time of the bare 2DEG, τ^{-1}. For all the disorder strength presented, $\tau^{-1} = 0, 0.1, 0.2, 0.3$ the system is in the topological phase. Each plot here corresponds to a single disorder realization. (b) The maximal eigenvalue of the zero-frequency transmission probability matrix, $T(\omega = 0)$, for the three disorder strength values in the topological phase. (c) The profile of the local density of states, integrated along the y direction, $\rho(x) \int dy \mathcal{N}(\omega = 0, x, y)$, for the different disorder strengths. The system's parameter are the same as in Fig. (1) of the main text, $E_{Z,J} = 1$ and $\phi = \pi$.

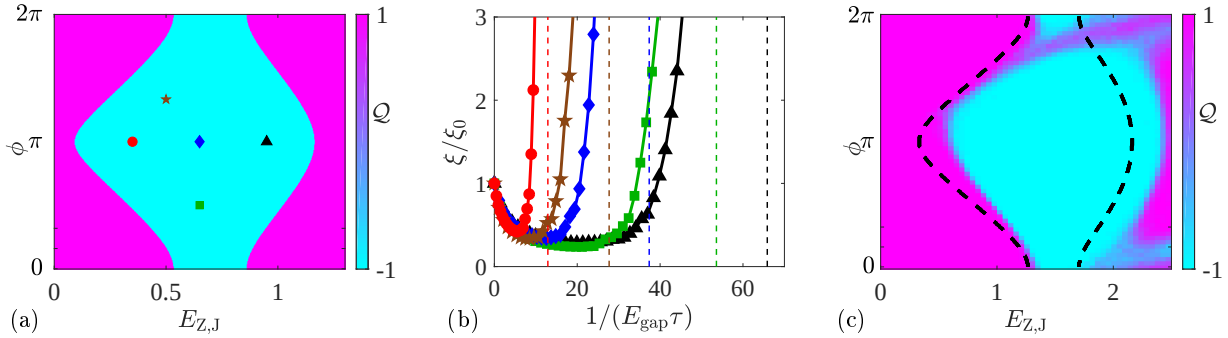

Figure 2. Results for different parameters. (a) The topological (blue) and trivial (pink) regions in the ϕ–B plane for a clean system, for $E_{so} = m_e\alpha^2/2 = 1$, $\Delta_0 = 1$, $\mu_J = \mu_{SC} = 0.5$, $E_{Z,SC} = 0$, $l_{so} = 1/m_e\alpha = 0.2W$, $W_{sc} = W$ (b) The Majorana localization length, ξ, as a function of the disorder-induced inverse mean free time, τ^{-1}, for different points inside the topological phase [see markers in (a)]. In (b), τ is normalized by the overall gap in the clean system, E_{gap}, which is 0.035, 0.033, 0.039, 0.022, and 0.029 for the red, brown, blue, green and black plots, respectively. (c) Phase diagram for chemical potential $\mu_J = \mu_{SC} = 1$, and junction width, $W = 2.5l_{so}$, for disorder strength, $\tau^{-1} = 0.5$. The reset of the system parameters are unchanged. The phase boundaries in the case of the corresponding clean system are shown in a black dashed line.

as in Fig. 1 of the main text. The topological invariant, $\mathcal{Q} = \det[r(0)]$, is shown for a disorder strength of $\tau^{-1} = 0.5$. The black dashed line represents the phase boundaries in the case of the clean system with the same parameters. Interestingly, for some magnetic fields, $E_{Z,J}$, and phase biases, ϕ, disorder drives the system from the trivial phase to the topological phase. A similar effect was previously observed in Refs. [8, 9].

II. THE ANALYSIS OF THE LINEARIZED MULTI-CHANNEL MODEL

In the main text we have studied a linearized low-energy model describing a disordered multi-channel superconductor, Eq. (2), and performed a perturbative analysis of the disorder, which resulted in new effective pairing potentials, Eq. (5). In this section we explain how this model can arise from a microscopic model, such as the planar JJ, Eq. (1) of the main text, and provide details regarding the calculation of the self energy which yielded the expression for the effective pairing potentials.

A. Origin of the model

We start from the 2d model of Eq. (1) of the main text, and separate the system to two parts: the normal part which is the strip defined by $|y| < W/2$, and the superconducting part, $|y| > W/2$. Following the Bardeen tunneling-

Hamiltonian approach [10], we then write the overall Hamiltonian as a combination of the three terms, describing the normal part, the SC part, and the coupling between them,

$$H = H_{\rm N} + H_{\rm SC} + H_{\rm N-SC}, \tag{6}$$

where $H_{\rm N}$ ($H_{\rm SC}$) is the Hamiltonian obtained by imposing hard-wall boundary conditions for $|y| > W/2$ ($|y| < W/2$). This treatment is valid when the normal reflection at the N-S interfaces ($y = \pm W/2$) is strong, such that the normal part as weakly coupled to the SC. This is the case, in particular, for the high-momentum modes as they impinge upon the N-S interface at large angles. Regardless of the above considerations, our numerical analysis shows that the qualitative conclusions drawn from the low-energy model of Eq. (2) of the main text hold much more generally.

We write the normal part, $H_{\rm N}$, as a combination as two terms,

$$H_{\rm N} = \int {\rm d}x \int_{-W/2}^{W/2} {\rm d}y \Psi^\dagger(x,y) \left[\mathcal{H}_{\rm N}^0(x,y) + \mathcal{H}_{\rm N}^{\rm dis}(x,y)\right] \Psi(x,y), \tag{7}$$

where $\mathcal{H}_{\rm N}^0$ describes the system in the clean limit, and $\mathcal{H}_{\rm N}^{\rm dis} = U(x,y)\tau_z$ is the part coming from disorder. Our treatment of the system is composed of two steps: (i) first we solve for $\mathcal{H}_{\rm N}^0$, and (ii) the disorder term and the induced superconductivity are then projected onto the basis diagonalizing $\mathcal{H}_{\rm N}^0$.

The clean part of the Hamiltonian, $\mathcal{H}_{\rm N}^0$, is generally solved by a set of eigenstates,

$$\vec{\varphi}_{\nu,k_x}(x,y) = \frac{e^{ik_x x}}{\sqrt{2\pi}} \cdot \begin{pmatrix} \eta^{\uparrow}_{\nu,k_x}(y) \\ \eta^{\downarrow}_{\nu,k_x}(y) \end{pmatrix}, \tag{8}$$

with corresponding eigen-energies, E_{ν,k_x}, and $\nu = 1, 2, \ldots, \infty$. Here, k_x is the momentum in the x direction, while ν labels the transverse channels.

1. *Reflection Symmetry*

The clean part of the Hamiltonian obeys the following symmetry,

$$\sigma_x \mathcal{H}_{\rm N}^0(-x,y)\sigma_x = \mathcal{H}_{\rm N}^0(x,y), \tag{9}$$

as can be checked by setting $U(x,y) = 0$ in Eq. (1) of the main text. The eigenstates can therefore be chosen to obey

$$\eta^s_{\nu,-k_x}(y) = \sum_{s'=\uparrow,\downarrow} \sigma^x_{ss'} \eta^{s'}_{\nu,k_x}(y). \tag{10}$$

2. *Conducting channels*

Depending on the chemical potential, some of the bands labeled by ν will cross zero energy, $E_{\nu,k_x} = 0$, for some momentum k_x. Due to the above reflection symmetry, these momenta will come in opposite-momentum pairs (except for potentially a single Fermi point at , which can occur when the chemical potential is at the bottom of one of the bands). The number of bands crossing zero energy, N, defines the number of conducting channels in the model. Correspondingly, we label the Fermi momenta by $k_{{\rm F},n}$, where $n = \pm 1, \ldots, \pm N$, and where $k_{{\rm F},-n} = -k_{{\rm F},n}$. Below we will be interested only in the modes having momentum near $k_{{\rm F},n}$.

3. *Projection and Linearization*

We first project the disorder part of the Hamiltonian onto the new basis. To this end, we first make the transformation

$$\hat{\psi}_s(x,y) = \int {\rm d}k e^{ik_x x} \sum_{\nu=1}^{\infty} \eta^s_{\nu,k_x}(y) \hat{a}_{\nu,k_x}, \tag{11}$$

where by definition, $\hat{a}_{\nu,k_x}$ creates an electron in the state described by $\vec{\varphi}_{\nu,k_x}(x,y)$. Setting in Eq. (7), one then has

$$H_{\rm N} = \sum_{\nu,k_x} E_{\nu,k_x}\hat{a}^\dagger_{n,k_x}\hat{a}_{n,k_x} + \int {\rm d}x \sum_{k_x,k'_x} e^{i(k'_x-k_x)x} \sum_{\nu,\nu'=1}^{\infty}\sum_s \int_{-W/2}^{W/2} {\rm d}y U(x,y)[\eta^s_{\nu,k_x}(y)]^*\eta^s_{\nu',k'_x}(y)\hat{a}^\dagger_{\nu,k_x}\hat{a}_{\nu',k'_x}. \tag{12}$$

Since we are concerned only with the low-energy modes, we can project out all the bands not crossing the Fermi energy. Out of the sum over ν, this leaves us only with a sum over $n = \pm 1, \ldots, \pm N$. Furthermore, we can limit the integral over k_x to momenta close to the Fermi points, $k_{{\rm F},n}$. This is done by defining the fields living close to the Fermi momenta, $\hat{a}_{n,k_{{\rm F},n}+q} \equiv \hat{\phi}_{n,q}$, where $q \in [-\Lambda, \Lambda]$. Finally, if the bottom of all the bands is far enough from the Fermi energy (which we shall assume to be the case), then we can approximate the dispersions of the modes near the Fermi points by $E_{n,k_x} \simeq \partial_{k_x} E_{n,k_x}|_{k_{{\rm F},n}} \cdot (k_x - k_{{\rm F},n}) \equiv v_n(k_x - k_{{\rm F},n})$, and take $\Lambda \to \infty$. Note also that due to the symmetry, Eq. (10), one has $v_{-n} = -v_n$. Applying the above procedure to Eq. (12), one has

$$\begin{aligned} H_{\rm N} &\simeq \sum_{n=\pm 1}^{\pm N}\int {\rm d}q v_n q \hat{\phi}^\dagger_{n,q}\hat{\phi}_{n,q} + \int {\rm d}x \int {\rm d}q \int {\rm d}q' e^{i(q'-q)x} \sum_{m,n=\pm 1}^{\pm N}\sum_s \int_{-W/2}^{W/2} {\rm d}y U(x,y)[\eta^s_{m,k_{{\rm F},m}}(y)]^*\eta^s_{n,k_{{\rm F},n}}(y)\hat{\phi}^\dagger_{m,q}\phi_{n,q'} \\ &= \sum_{n=\pm 1}^{\pm N}\int {\rm d}x v_n \hat{\phi}^\dagger_n(x)(-iv_n\partial_x)\hat{\phi}_n(x) + \int {\rm d}x \sum_{m,n=\pm 1}^{\pm N} V_{mn}(x)\hat{\phi}^\dagger_m(x)\hat{\phi}_n(x), \end{aligned} \tag{13}$$

where we have defined

$$V_{mn}(x) = \sum_s \int_{-W/2}^{W/2} {\rm d}y U(x,y)[\eta^s_{m,k_{{\rm F},m}}(y)]^*\eta^s_{n,k_{{\rm F},n}}(y). \tag{14}$$

Finally, we account for the coupling to the superconducting region. At least in principle, one can integrate out the degrees of freedom of the SC region [11, 12]. This will result in *induced* pairing potential operating on the modes living in the normal region,

$$H^{\rm ind}_{\rm N} = \int {\rm d}x \sum_{m,n=\pm 1}^{\pm N} \Delta_{mn}\hat{\phi}^\dagger_m(x)\hat{\phi}^\dagger_n(x). \tag{15}$$

Importantly, only pairing between modes of opposite momenta will open a gap at the Fermi energy. Assuming the Fermi momenta, $k_{{\rm F},m}$, are not degenerate (this will generally be the case when breaking SU(2) symmetry), we can therefore omit all the pairing terms except for $\Delta_{m,-m} \equiv \Delta_m$. Combining with Eq. (13), the Hamiltonian describing the overall system at low energies is given by

$$H \simeq \int {\rm d}x \left\{ \sum_{m=\pm 1}^{\pm N} \left[v_m \hat{\phi}^\dagger_m(x)(-iv_m\partial_x)\hat{\phi}_m(x) + \Delta_m \hat{\phi}^\dagger_m(x)\hat{\phi}^\dagger_{-m}(x)\right] + \sum_{m,n=\pm 1}^{\pm N} V_{mn}(x)\hat{\phi}^\dagger_m(x)\hat{\phi}_n(x)\right\}, \tag{16}$$

which is the Hamiltonian introduced in Eq. (2) of the main text.

4. *Properties of the disorder term*

The new effectively-1D disorder potential, $V_{mn}(x)$, is manifestly Hermitian, $V^*_{mn}(x) = V_{nm}(x)$. Furthermore, due to the symmetry, Eq. (10), it obeys $V_{-m,-n}(x) = V_{mn}(x)$. From Eq. (14), we can obtain the correlations of $V_{mn}(x)$, which are given by

$$\langle V_{mn}(x)V_{mn}(x')\rangle = \gamma_{mn}\delta(x-x'), \tag{17}$$

where we defined

$$\gamma_{mn} \equiv \gamma \int_{-W/2}^{W/2} {\rm d}y \left[\vec{\eta}^\dagger_{m,k_{{\rm F},m}}(y)\vec{\eta}_{n,k_{{\rm F},n}}(y)\right]^2, \tag{18}$$

and where we have used the fact that $\langle U(x,y)U(x',y')\rangle = \gamma\delta(\boldsymbol{r}-\boldsymbol{r}')$. Notice also that

$$\langle V_{mn}(x)V_{nm}(x')\rangle = |\gamma_{mn}|\delta(x-x'). \tag{19}$$

B. Derivation of the self energy

1. Gauging out the diagonal scattering terms

Starting from the low-energy Hamiltonian, Eq. (2) of the main text, we define the fields

$$\tilde{\phi}_m(x) = \phi_m(x) e^{\frac{i}{v_m}\int_{-\infty}^{x} \mathrm{d}x_1 V_{mm}(x_1)}. \tag{20}$$

Inserting this definition into Eq. (2) of the main text, we arrive at an identical Hamiltonian, except that now intra-mode scattering is absent,

$$H = \int \mathrm{d}x \left(\sum_{m=\pm 1}^{\pm N} \left\{ v_m \tilde{\phi}_m^\dagger(x)(-i\partial_x)\tilde{\phi}_m(x) + \frac{1}{2}\left[\Delta_m \tilde{\phi}_m^\dagger(x)\tilde{\phi}_{-m}^\dagger(x) + \text{h.c.}\right]\right\} + \sum_{m,n=\pm 1}^{\pm N} e^{i(k_{\mathrm{F},m}-k_{\mathrm{F},n})x}\tilde{V}_{mn}(x)\phi_m^\dagger(x)\phi_n(x)\right), \tag{21}$$

where,

$$\tilde{V}_{mn}(x) \equiv \begin{cases} V_{mn}(x) e^{i\int_{-\infty}^{x}\mathrm{d}x_1\left[\frac{1}{v_m}V_{mm}(x_1) - \frac{1}{v_n}V_{nn}(x_1)\right]}, & m \neq n \\ 0, & m = n, \end{cases} \tag{22}$$

and we have used the fact that $V_{mm}(x) = V_{-m,-m}(x)$. To leading order in the disorder strength, the correlations of the new disorder term are unaltered,

$$\langle V_{mn}(x) V_{mn}(x') e^{i\int_{x'}^{x}\mathrm{d}x_1\left[\frac{1}{v_m}V_{mm}(x_1) - \frac{1}{v_n}V_{nn}(x_1)\right]}\rangle \simeq \gamma_{mn}\delta(x-x') + \mathcal{O}(V^4). \tag{23}$$

2. Born approximation

We begin by rewriting the Hamiltonian in a BdG form

$$H = \int \mathrm{d}x \sum_{mn} \left(\tilde{\phi}_m^\dagger(x), \tilde{\phi}_{-m}(x)\right) \mathcal{H}_{mn}(x) \begin{pmatrix} \tilde{\phi}_n(x) \\ \tilde{\phi}_{-n}^\dagger(x) \end{pmatrix}, \tag{24}$$

where $\mathcal{H}_{mn}(x) = \mathcal{H}^0_{mn}(x) + \mathcal{V}_{mn}(x)$,

$$\mathcal{H}^0_{mn}(x) = \begin{pmatrix} -iv_m\partial_x & \Delta_m \\ \Delta_m^* & -iv_{-m}\partial_x \end{pmatrix}\delta_{mn} \quad ; \quad \mathcal{V}_{mn}(x) = \begin{pmatrix} \tilde{V}_{mn}(x) & 0 \\ 0 & -\tilde{V}_{n,m}(x) \end{pmatrix} e^{ik_{mn}x}, \tag{25}$$

where $k_{mn} = k_{\mathrm{F},m} - k_{\mathrm{F},n}$.

The diagonal elements of the disorder-averaged Green function are given by

$$\begin{aligned} \langle G_{mm}(x,x')\rangle = G^0_{mm}(x,x') &+ \int \mathrm{d}x_1 G^0_{mm}(x,x_1)\langle \mathcal{V}_{mm}(x_1)\rangle G^0_{mm}(x_1,x') \\ &+ \int \mathrm{d}x_1 \int \mathrm{d}x_2 \sum_n G^0_{mm}(x,x_1)\left\langle \mathcal{V}_{mn}(x_1) G^0_{nn}(x_1,x_2)\mathcal{V}_{nm}(x_2)\right\rangle G^0_{mm}(x_2,x') + \dots \end{aligned} \tag{26}$$

Using Eqs. (17-19), and defining the phase α_{mn} through $\gamma_{mn} = |\gamma_{mn}|\exp(i\alpha_{mn})$, we can write

$$\begin{aligned} \langle G_{mm}(x,x')\rangle &= G^0_{mm}(x,x') + \int \mathrm{d}x_1 \sum_n |\gamma_{mn}| G^0_{mm}(x,x_1) e^{i\frac{\alpha_{mn}}{2}\tau_z}\tau_z G^0_{nn}(x_1,x_1)\tau_z e^{-i\frac{\alpha_{mn}}{2}\tau_z} G^0_{mm}(x_1,x') + \dots = \\ &= \int \frac{\mathrm{d}q}{2\pi} e^{iq(x-x')} G^0_{mm}(q)\left\{1 + \sum_n |\gamma_{mn}| e^{i\frac{\alpha_{mn}}{2}\tau_z}\tau_z \int \frac{\mathrm{d}q'}{2\pi} G^0_{nn}(q')\tau_z e^{-i\frac{\alpha_{mn}}{2}\tau_z}\cdot G^0_{mm}(q) + \dots\right\}. \end{aligned} \tag{27}$$

From this one extracts the self energy to leading order,

$$\begin{aligned} \Sigma_m(q) &= \sum_n |\gamma_{mn}| e^{i\frac{\alpha_{mn}}{2}\tau_z}\tau_z \int \frac{\mathrm{d}q'}{2\pi} G^0_{nn}(q')\tau_z e^{-i\frac{\alpha_{mn}}{2}\tau_z} = -\sum_n \frac{|\gamma_{mn}|}{2v_n} e^{i\frac{\alpha_{mn}}{2}\tau_z}\tau_z e^{i\arg(\Delta_n)}\tau_x\tau_z e^{-i\frac{\alpha_{mn}}{2}\tau_z} \\ &= \sum_n \frac{|\gamma_{mn}|}{2v_n} e^{i[\arg(\Delta_n)+\alpha_{mn}]\tau_z}\tau_x, \end{aligned} \tag{28}$$

where we have used the expression for $G^0_{nn}(q')$ given in Eq. (3) of the main text. At low energies one can construct an effective Hamiltonian describing the m-th channel, $\mathcal{H}^{\rm eff}_{mm}(q) = \mathcal{H}^0_{mm}(q) + \Sigma_m(q)$, where $\mathcal{H}^0_{mm}(q)$ is the Fourier space representation of $\mathcal{H}^0_{mm}(x)$ defined in Eq. (25). This then defines an effective pairing potential,

$$\Delta^{\rm eff}_m = \Delta_m + \frac{1}{2}\sum_n \frac{1}{\tau_{mn}} e^{i[\arg(\Delta_n)+\alpha_{mn}]}, \tag{29}$$

as appearing in Eq. (5) of the main text.

3. *Effective time-reversal symmetry*

In the case of the planar Josephson junction, the expressions for the self energy and the effective pairing potentials, Eqs. (28) and (29), can be simplified thanks to another symmetry. While the system breaks the usual time-reversal symmetry due to the presence of a magnetic field, it nevertheless obeys (in the clean limit) an anti-unitary symmetry, given by [13]

$$[\mathcal{H}^0_{\rm N}(x,-y)]^* = \mathcal{H}^0_{\rm N}(x,y). \tag{30}$$

One can therefore choose the eigenstates to obey,

$$\eta^s_{\nu,-k_x}(y) = [\eta^s_{\nu,k_x}(-y)]^*, \tag{31}$$

and together with the symmetry of Eq. (10) one has $\eta^s_{\nu,k_x}(y) = \sum_s \sigma^x_{ss'}[\eta^{s'}_{\nu,k_x}(-y)]^*$.

From this one can infer that γ_{mn} is real and positive,

$$\gamma^*_{mn} = \gamma\int_{-W/2}^{W/2} {\rm d}y \left[\sum_{s,s',s''} \sigma^x_{ss'}\sigma^x_{ss''}[\eta^{s'}_{m,k_{{\rm F},m}}(-y)]^*\eta^{s''}_{n,k_{{\rm F},n}}(-y)\right]^2 = \gamma\int_{-W/2}^{W/2} {\rm d}y \left[\sum_s [\eta^s_{m,k_{{\rm F},m}}(y)]^*\eta^s_{n,k_{{\rm F},n}}(y)\right]^2 = \gamma_{mn}. \tag{32}$$

III. SOLUTION BY MAPPING TO A NORMAL DISORDERED WIRE

In the main text we have used Eq. (5) to study two special cases: (i) the single-channel p-wave SC, and (ii) the single-(spinful)-channel s-wave. While Eq (5) of the main text was derived under the assumption of weak disorder, we here show that the results for the above special cases are exact. Inspired by the approach of Rieder *et al.* [14], we use a mapping of these superconducting systems, at zero energy, to a disordered normal-metal wire, whose properties have been previously studied [15–17].

A. The (spinless) single-channel p-wave superconductor

The linearized Hamiltonian for single-channel p-wave superconductor in the presence of short-range disorder is given by

$$H_{\rm p} = \int {\rm d}x\Big\{ -iv\left[R^\dagger(x)\partial_x R(x) - L(x)^\dagger\partial_x L(x)\right] + \Delta\left[R^\dagger(x)L^\dagger(x) + L(x)R(x)\right] + V(x)\left[R^\dagger(x)R(x) + L^\dagger(x)L(x)\right] + \\ + \left[V(x)e^{2ik_{\rm F}x}R^\dagger(x)L(x) + {\rm h.c.}\right]\Big\}. \tag{33}$$

In terms of the notation used in Eq. (2) of the main text, $\phi_1(x) = R(x)$, and $\phi_{-1}(x) = L(x)$. The above Hamiltonian can be written in the BdG form, $H_{\rm p} = \frac{1}{2}\int {\rm d}x \Phi^\dagger(x)\mathcal{H}_{\rm p}(x)\Phi(x)$,

$$\mathcal{H}_{\rm p}(x) = -iv\partial_x\sigma_z + V(x)\tau_z + V'(x)\sigma_x\tau_z - V"(x)\sigma_y - \Delta\tau_y\sigma_y, \tag{34}$$

where here $\Phi^\dagger(x) = [R^\dagger(x), R(x), L^\dagger(x), L(x)]$, and $V'(x) = V(x)\cos(2k_{\rm F}x)$, $V"(x) = V(x)\sin(2k_{\rm F}x)$. The disorder potential $V(x)$ is described by the correlations $\langle V(x)V(x')\rangle = \gamma_{\rm p}\delta(x-x')$.

The localization length, at a given energy, can be obtained from the transfer matrix, $M(x,\varepsilon)$, defined as the 4×4 matrix obeying

$$\Phi(x,\varepsilon) = M(x,\varepsilon)\cdot\Phi(0,\varepsilon), \tag{35}$$

where $\Phi(x,\varepsilon)\equiv\int \mathrm{d}t\Phi(x,t)\exp(-i\varepsilon t)$, and propagation in time is according to $H_{\rm p}$. The localization length is related to the transfer matrix through the eigenvalues of $M^\dagger M$, which in the localized phase take the form $\exp(\pm 2\lambda_i L)$ when $L\to\infty$, where $\{\lambda_i\}$ are the so-called Lyapunov exponents [18, 19]. The localization length is then determined by the slowest decaying exponent, $\xi = 1/\max\{\lambda_i\}$

Writing the Hamiltonian, Eq. (34), as $\mathcal{H}_{\rm p} = -iv\sigma_z(\partial_x + \mathcal{H}_1)$, the Schrödinger equation for $\Phi(x,\varepsilon)$ takes the form $\partial_x\Phi(x,\varepsilon) = (i\sigma_z\varepsilon/v - \mathcal{H}_1)\Phi(x,\varepsilon)$, which is solved by $\Phi(x,\varepsilon) = \mathcal{T}_x\exp[i\sigma_z\varepsilon x/v - \int_0^x \mathrm{d}x'\mathcal{H}_1(x')]\Phi(0,\varepsilon)$, where $\mathcal{T}_x$ is the path ordering operator. Namely the zero-energy transfer matrix from one side of the system to the other is given by

$$M(L,\varepsilon=0) = \mathcal{T}_x\exp\left\{\frac{1}{v}\int_0^L \mathrm{d}x\left[-iV(x)\sigma_z\tau_z + V'(x)\sigma_y\tau_z + V"(x)\sigma_x + \Delta\sigma_x\tau_y\right]\right\}. \tag{36}$$

The last term in the exponent, $\Delta\tau_y\sigma_x$, commutes with all other terms. Therefore, the transfer matrix decomposes into two 2×2 blocks, $M_\pm$, where the $\pm$ refers to the eigenvalue of $\tau_y\sigma_x$. These blocks are given by,

$$M_\pm(L,\varepsilon=0) = M_{\rm N}(L,\varepsilon=0)e^{\pm\Delta L/v} \tag{37}$$

where $M_{\rm N}(L,\varepsilon)$ is the transfer matrix for a single-channel normal wire of linear dispersion.

The problem of a normal disordered wire has been solved elsewhere [15–17], and the resulting eigenvalues of $M_{\rm N}^\dagger(L,0)M_{\rm N}(L,0)$ read $e^{\pm 2\lambda_{\rm N}L}$, where $\langle\lambda_{\rm N}\rangle \underset{L\to\infty}{\to} 1/2l$ and its variance goes to zero. From Eq. (37) we then conclude that the four eigenvalues of $M^\dagger(L,0)M(L,0)$ are given by $e^{\pm 2(\lambda_{\rm N}\pm\Delta/v)L}$, which means that the zero-energy localization length for the p-wave SC reads

$$\frac{1}{\xi_{\rm p}} = \left|\frac{1}{\xi_{\rm p}^0} - \frac{1}{2l}\right|, \tag{38}$$

where $\xi_{\rm p}^0 = v/\Delta$, in accordance with the result shown below Eq. (6) of the main text. While that result was obtained from a perturbative weak-disorder treatment, the calculation leading to Eq. (38) is exact (within the linearized model).

B. The (spinful) single-channel s-wave superconductor

We now move on to a single spinful channel s-wave SC. The linearized Hamiltonian for such a system is given by

$$\begin{aligned} H_{\rm s} = \int \mathrm{d}x\Big(\sum_{s=\uparrow\downarrow}\left\{-iv\left[R_s^\dagger(x)\partial_x R_s(x) - L_s^\dagger(x)\partial_x L_s(x)\right] + V(x)\left[R_s^\dagger(x)R_s(x) + L_s^\dagger(x)L_s(x)\right] + \left[V(x)R_s^\dagger(x)L_s(x) + \text{h.c.}\right]\right\} \\ + \Delta\left[R_\uparrow^\dagger(x)L_\downarrow^\dagger(x) + L_\uparrow^\dagger(x)R_\downarrow^\dagger(x) + \text{h.c.}\right]\Big). \end{aligned} \tag{39}$$

We can write it in the BdG form $H_{\rm s} = \int \mathrm{d}x\Phi^\dagger(x)\mathcal{H}_{\rm s}(x)\Phi(x)$,

$$\mathcal{H}_{\rm s}(x) = -iv\partial_x\sigma_z + V(x)\tau_z + V'(x)\sigma_x\tau_z - V"(x)\sigma_y + \Delta\tau_x\sigma_x. \tag{40}$$

where this time $\Phi^\dagger(x) = [R_\uparrow^\dagger(x), R_\downarrow(x), L_\uparrow^\dagger(x), L_\downarrow(x)]$. This Hamiltonian resembles the p-wave BdG Hamiltonian of Eq. (34), except for the matrix structure of the pairing term, Δ. This difference comes from the fact that in the p-wave case, the pairing potential switches sign when going from positive to negative momenta. Notice that even though the s-wave SC is spinful, we could defined the BdG matrix, $\mathcal{H}_{\rm s}$, such that it would have the same size as $\mathcal{H}_{\rm p}$. This is possible only because the disorder term in Eq. (39) does not mixes opposite spins.

We can obtain an expression for the transfer matrix in exactly the same way as we did above for the p-wave case [see Eq. (36)]. This results in

$$M(L,\varepsilon=0) = \mathcal{T}_x\exp\left\{\frac{1}{v}\int_0^L \mathrm{d}x\left[-iV(x)\sigma_z\tau_z + V'(x)\sigma_y\tau_z + V"(x)\sigma_x + \Delta\sigma_y\tau_x\right]\right\}. \tag{41}$$

Unlike in the p-wave case, this time the pairing term, $\Delta\tau_x\sigma_y$, does *not* commute with the rest of the terms in the exponent. Nevertheless, all terms in the exponent still commute with $\tau_y\sigma_x$. We can therefore decompose $M(L,0)$ into two blocks by going to the basis which diagonalizes $\tau_y\sigma_x$. This is done by $\tilde{M}(L,0)=\mathcal{U}^\dagger M(L,0)\mathcal{U}=M_+\oplus M_-$, where $\mathcal{U}=\frac{1}{2}\left[1+\tau_z+\sigma_x(1-\tau_z)\right]e^{i\frac{\pi}{4}\tau_x}$, and where

$$\tilde{M}_\pm=\mathcal{T}_x\exp\left\{\frac{1}{v}\int_0^L \mathrm{d}x\left[-iV(x)\sigma_z+V'(x)\sigma_y+V"(x)\sigma_x\pm\Delta\sigma_z\right]\right\}. \tag{42}$$

In the absence of Δ, the matrices $\tilde{M}_\pm$ both correspond again to the transfer matrix of single-channel normal disordered wire (with linear dispersion). Importantly, we notice that Δ enters in Eq. (42) as an imaginary energy, $V(x)\to V(x)\pm i\Delta$, namely

$$\tilde{M}_\pm=M_{\rm N}(L,\varepsilon=\pm i\Delta). \tag{43}$$

Namely, the zero-energy s-wave transfer matrix is mapped to two copies of a normal disordered wire at finite energy, with the analytic continuation, $\varepsilon\to\pm i\Delta$.

To perform the analytic continuation, we first use the Friedel sum rule. For the case of a single-channel normal wire, it relates the reflection amplitude for a system with *open boundary conditions*, $r_{\rm obc}(L,\varepsilon)=e^{i\varphi(\varepsilon,L)}$, to the density of states per unit length, $\nu(\varepsilon)$, through

$$\nu(\varepsilon)=\lim_{L\to\infty}\frac{1}{2\pi L}\frac{\partial\varphi(\varepsilon,L)}{\partial\varepsilon}, \tag{44}$$

where $r_{\rm obc}(L,\varepsilon)$ is the reflection for an electron incident at $x=0$, with a boundary condition $\Phi(x=L)=0$. For the linearized model of the disordered wire, the density of states (in the thermodynamic limit) is constant, $\nu=1/2\pi v$, yielding

$$\varphi(\varepsilon,L)=\varphi_0(L)+\varepsilon L/v, \tag{45}$$

The above reflection amplitude, $r_{\rm obc}$, is related to the transfer matrix through

$$\begin{pmatrix} r_{\rm obc}\\ 1\end{pmatrix}=M_{\rm N}(L,\varepsilon)\begin{pmatrix}1\\1\end{pmatrix}. \tag{46}$$

We write the transfer matrix of the normal wire using its polar decomposition [18, 19],

$$M_{\rm N}(L,\varepsilon)=\begin{pmatrix}e^{i\alpha}&0\\0&e^{-i\alpha}\end{pmatrix}\begin{pmatrix}\cosh(\mu)&\sinh(\mu)\\\sinh(\mu)&\cosh(\mu)\end{pmatrix}\begin{pmatrix}e^{i\beta}&0\\0&e^{-i\beta}\end{pmatrix}, \tag{47}$$

where the parameter μ is related to the Lyapunov exponent by $\mu=\lambda_N L$, when $L\to\infty$. From Eqs. (46) and (47) we then conclude that $r_{\rm obc}=e^{2i\alpha}$, namely $\alpha(L,\varepsilon)\underset{L\to\infty}{\to}\alpha_0(L)+\varepsilon L/2v$. Applying the same arguments for an electron incident towards the left at $x=L$, with open boundary conditions at $x=0$, one concludes that $\beta(L,\varepsilon)\underset{L\to\infty}{\to}\beta_0(L)+\varepsilon L/2v$.

We can now perform the analytic continuation,

$$M_{\rm N}(L,\varepsilon\to i\Delta)=\begin{pmatrix}e^{i\alpha_0}&0\\0&e^{-i\alpha_0}\end{pmatrix}\begin{pmatrix}e^{-\Delta L/v}\cosh(L/2l)&\sinh(L/2l)\\\sinh(L/2l)&e^{\Delta L/v}\cosh(L/2l)\end{pmatrix}\begin{pmatrix}e^{i\beta_0}&0\\0&e^{-i\beta_0}\end{pmatrix}. \tag{48}$$

Finally, one computes the eigenvalues of $M_{\rm N}(L,i\Delta)[M_{\rm N}(L,i\Delta)]^\dagger$, which are given by

$$e^{\pm2\cosh^{-1}[\cosh(L/2l)\cosh(\Delta L/v)]}\underset{L\to\infty}{\longrightarrow}e^{\pm2(1/2l+\Delta/v)L}.$$

A similar results is obtained for $M_{\rm N}(L,-i\Delta)[M_{\rm N}(L,-i\Delta)]^\dagger$, so that altogether we get

$$\frac{1}{\xi_{\rm s}}=\frac{1}{\xi_{\rm s}^0}+\frac{1}{2l}, \tag{49}$$

in accordance with the result of Eq. (7) of the main text.

[1] D. S. Fisher and P. A. Lee, Phys. Rev. B **23**, 6851 (1981).

[2] S. Iida, H. A. Weidenmüller, and J. Zuk, Ann. Phys. **200**, 219 (1990).
[3] P. A. Lee and D. S. Fisher, Phys. Rev. Lett. **47**, 882 (1981).
[4] A. R. Akhmerov, J. P. Dahlhaus, F. Hassler, M. Wimmer, and C. W. J. Beenakker, Phys. Rev. Lett. **106**, 057001 (2011).
[5] I. C. Fulga, F. Hassler, A. R. Akhmerov, and C. W. J. Beenakker, Phys. Rev. B **83**, 155429 (2011).
[6] A. Kitaev, Phys. Usp. **44**, 131 (2001).
[7] A. C. Potter and P. A. Lee, Phys. Rev. B **83**, 094525 (2011).
[8] I. Adagideli, M. Wimmer, and A. Teker, Phys. Rev. B **89**, 144506 (2014).
[9] F. Pientka, A. Romito, M. Duckheim, Y. Oreg, and F. von Oppen, New J. Phys. **15**, 025001 (2013).
[10] J. Bardeen, Phys. Rev. Lett. **6**, 57 (1961).
[11] J. Alicea, Rep. Prog. Phys. **75**, 076501 (2012).
[12] A. Haim, K. Wölms, E. Berg, Y. Oreg, and K. Flensberg, Phys. Rev. B **94**, 115124 (2016).
[13] F. Pientka, A. Keselman, E. Berg, A. Yacoby, A. Stern, and B. I. Halperin, Phys. Rev. X **7**, 021032 (2017).
[14] M.-T. Rieder, P. W. Brouwer, and I. Adagideli, Phys. Rev. B **88**, 060509 (2013).
[15] B. I. Halperin, Advances in Chemical Physics **13**, 123 (1967).
[16] O. Dorokhov, JETP Lett **36**, 318 (1982).
[17] P. Mello, P. Pereyra, and N. Kumar, Annals of Physics **181**, 290 (1988).
[18] C. W. J. Beenakker, Rev. Mod. Phys. **69**, 731 (1997).
[19] F. Evers and A. D. Mirlin, Rev. Mod. Phys. **80**, 1355 (2008).